An approach for mechanical property optimization of fused deposition modeling with polylactic acid via design of experiments

AQ: au

Ali P. Gordon, Jonathan Torres, Matthew Cole, Allen Owji and Zachary DeMastry
Department of Mechanical and Aerospace Engineering, University of Central Florida, Orlando, Florida, USA

Abstract

Purpose – This paper aims to present the influences of several production variables on the mechanical properties of specimens manufactured using fused deposition modeling (FDM) with polylactic acid (PLA) as a media and relate the practical and experimental implications of these as related to stiffness, strength, ductility and generalized loading.

Design/methodology/approach – A two-factor-level Taguchi test matrix was defined to allow streamlined mechanical testing of several different fabrication settings using a reduced array of experiments. Specimens were manufactured and tested according to ASTM E8/D638 and E399/D5045 standards for tensile and fracture testing. After initial analysis of mechanical properties derived from mechanical tests, analysis of variance was used to infer optimized production variables for general use and for application/load-specific instances.

Findings – Production variables are determined to yield optimized mechanical properties under tensile and fracture-type loading as related to orientation of loading and fabrication.

Practical implications – The relation of production variables and their interactions and the manner in which they influence mechanical properties provide insight to the feasibility of using FDM for rapid manufacturing of components for experimental, commercial or consumer-level use.

Originality/value – This paper is the first report of research on the characterization of the mechanical properties of PLA coupons manufactured using FDM by the Taguchi method. The investigation is relevant both in commercial and consumer-level aspects, given both the currently increasing utilization of 3D printers for component production and the viability of PLA as a renewable, biocompatible material for use in structural applications.

Keywords Optimization techniques, Rapid prototyping, Additive manufacturing, 3D printing, Fractional factorial, Fracture toughness

Paper type Research paper

1. Introduction

Rapid prototyping techniques have been advancing rapidly since the commercialization of the first method, stereolithography, in the late 1980s, which utilizes a laser to cure successive layers of a liquid polymer into the desired structure (Bártolo, 2011; Jacobs, 1992; Hopkinson and Dickens, 2001; Mellor *et al.*, 2014). Several rapid manufacturing technologies now exist which utilize various techniques and materials to construct components one layer at a time from a CAD file. Systems such as 3D printing and selective laser sintering use a polymer powder base which is then joined together layer-by-layer using either an injected binder or fused by laser heating, respectively (Bogue, 2013). In fused deposition modeling (FDM), the layers are created by the heating and deposition of a thermoplastic filament extruded through a motorized nozzle onto a platform.

It was the expiration of the original patents for FDM in 2009 which made rapid manufacturing technologies widely available to industry and individuals alike (Crump, 1992).

Rapid manufacturing is now accessible to broad audiences, but the processing-to-property relations are still not well-known. Thermoplastic extrusion FDM systems are typically less expensive and safer to maintain, as the powders and resins which other systems use can create hazardous environments for hardware and sometimes toxic air conditions for users, along with the high cost of maintaining expensive hardware such as lasers (McMains, 2005). These systems were also found to be the most suitable choice for home and small business use, via evaluation of some popular models of each type of technology using performance and cost criteria such as build time, system cost, dimensional accuracy and material usage and waste (Roberson *et al.*, 2013; Stanek *et al.*, 2012).

As such, with the growing popularity of FDM printer systems for consumer-level use, the mechanical evaluation of components produced in this fashion is of paramount interest. Fused deposition modeled parts have previously been evaluated for several different parameters, including dimensional accuracy and smoothness, compressive, tensile, flexural and impact strength (Lee *et al.*, 2007; Panda *et al.*, 2009; Zhang and Peng, 2012). Lee *et al.* (2007) observed that

Fused deposition modeling with polylactic acid
Ali P. Gordon et al.

Rapid Prototyping Journal
Volume 22 · Number 2 · 2016 · 000–000

the compressive strengths of FDM parts are 23.6 per cent higher in axially loaded specimens than in transverse specimens, thereby showing the effects of print orientation. Panda *et al.* (2009) showed the effects of processing properties; while decreasing layer thickness raises both tensile and flexural strength, increasing it improves impact strength. Traditionally, however, FDM studies such as those previously cited have focused around acrylonitrile butadiene styrene (ABS) components, rather than the more environmentally friendly and popular polylactic acid (PLA), which is used in many of the increasingly popular desktop printers. PLA is a biodegradable thermoplastic polymerized from natural lactic acid from natural sources such as corn (Ashby and Johnson, 2013). Some of the characteristics of bulk PLA are given in Table I. Though PLA has a larger strength and lower ductility than the traditional ABS, PLA is a sustainable thermoplastic alternative which addresses the problem of added waste from end-users manufacturing components at home and has similar characteristics as ABS. Parts produced via FDM from PLA have also been of high interest to the medical field, due to the biocompatibility of PLA for use in applications such as tissue engineering and implants custom-made per patient needs (Drummer *et al.*, 2012; Too *et al.*, 2002).

It is evident that there is a need to thoroughly evaluate the properties of PLA components produced via FDM, primarily in strength and fracture characteristics, so that they may continue to be successfully used for both industrial and general use. Complications arise, however, in testing these components, as the several different factors which affect print quality and strength of a component are affected by the multiple adjustable settings of the FDM machine. It has been shown that factors such as material extrusion temperature, T; component manufacturing orientation; and layer thickness, δ, strongly affect the strength and durability of components produced via FDM using ABS (Sood *et al.*, 2010). Combined with other commodity desktop printer settings, such as print speed and infill density, the number of experiments needed to evaluate the effects of each individual parameter on component strength and fracture behavior can quickly escalate. The Taguchi method of design of experiments (DoE) curtails extensive experimentation as encountered when using

a full factorial experiment (FFE) (Roy, 2001). Using the FFE method, the number of experiments necessary equals the number of levels tested for each factor raised to the number of factors; this means, for example, any arbitrary three-level four-factor experiment would require 3^4, or 81 experiments (Lee and Kuo, 2013). The Taguchi method allows for the selection of a partial factorial test matrix to test multiple factors with several levels at once and account for interactions between these with a minimum amount of experiments, which can later be analyzed using analysis of variance (ANOVA) (Roy, 2001; Wen *et al.*, 2009). With the three-level four-factor experiment previously mentioned, the L9 matrix can be utilized to reduce the original 81 experiments to just nine experiments, an 89 per cent reduction. The Taguchi method has been shown to be a valid approach for evaluating the effects of the different factors present in FDM, simplifying experimentation while evaluating multiple factor levels and their influence on component performance (Patel *et al.*, 2012; Sood *et al.*, 2011; Zhang and Peng, 2012).

ANOVA is a statistical process which evaluates the variance between individuals or groups of individuals to assess the effects of treatments (Girden, 1992; Montgomery, 2012). The use of ANOVA gives a statistical measure, F, which is the ratio of the between-group variance, or variance due to treatments, divided by the error, which is a result of within-group variance (Roberts and Russo, 1999). The variance, or mean square, is calculated as the sum of squares divided by the degrees of freedom. The mean square due to treatment can then be divided by the mean square of error to obtain an F value, which is useful in gauging the effect of each condition on the mean (Miller, 1997); in this situation, the F values can be used to gauge the effects of each processing parameter on the select material properties of interest:

$$F = \frac{\sum_{i=1}^{N} (x_i - \bar{x})^2}{\sum_{i=1}^{n} (n-1)\, \sigma_x^2} \cdot \frac{N-p}{p-1} \qquad (1)$$

where p is the total number of populations, n is the total number of samples within a population, N is the total number of observations and σ_x is the standard deviation of the samples.

These results establish a reference guide by which users can more intuitively determine which factors will affect their components and to what extent, allowing them to decide how best to tune their printer for maximum component performance, depending on their application. Moreover, the process established herein to determine these properties can be used to optimize collective or individual FDM properties for other platforms and materials, allowing users to optimize for whichever properties are desired given their own specialized circumstances and equipment.

In this study, DoE is applied to determine an experimental array by which several process settings, or factors, of a commodity FDM device can be evaluated without the need for full factorial testing. Results are analyzed using ANOVA to determine factor impact on tensile and fracture characteristics,

Table I Material properties of bulk polylactic acid as given by manufacturers and literature

Property	Unit	Value
Density, ρ	g/cm^3	1.24
Melting temperature, T_m	°C	130-230
Elongation at break	%	7.0
Elastic modulus, E	MPa	3,500
Shear modulus, G	MPa	1,287
Poisson's ratio, v	–	0.360
Yield strength, σ_y	MPa	70
Flexural strength, σ_f	MPa	106
Unnotched izod impact	J/m	195
Rockwell hardness	HR	88
Ultimate tensile strength, σ_{usd}	MPa	73

Sources: Jamshidian *et al.* (2010); Bijarimi *et al.* (2012); Clarinval and Halleux (2005); Ashby and Johnson (2013); Henton *et al.* (2005); Subhani (2011)

such as yield strength, σ_y; Young's modulus, E; and critical stress intensity factor, K_Q.

2. Experimental approach

Drawing out the mechanical properties of the candidate solid, PLA, is accomplished via experimental mechanics of materials. Standard methods such as fracture toughness testing, tensile testing and the like are ubiquitous, as they can be applied to monolithics, composites, metals, polymers, etc. Although the maturity of additive manufacturing materials has yet to reach the point where ASTM/ISO protocols have been established for testing, existing methods provide guidelines to establish the fractural and tensile properties of orthotropic PLA FDM components. Standards do exist, however, which set guidelines for general terminology and reporting, such as ISO/ASTM 52921.

Samples were manufactured using a common FDM desktop printer (MakerBot Replicator2), as it represents a commodity device for rapid manufacturing machines. This is a single extruder rapid prototype machine which uses a 1.75-mm PLA filament to produce components via FDM, which serves as an ideal representation of desktop FDM printers for small-scale production/prototyping. Temperature, T; print speed, s; infill direction, θ; relative density (or infill per cent), ρ; and layer thickness, δ, are the most common parameters which may be adjusted based on the object to be printed. The infill direction, which will be defined later, was adjusted using Skeinforge, a software addition which works in conjunction with the proprietary software of the printer and expands the available control level to a more advanced adjustability level.

The number of runs, or experiments, necessary was determined by the use of the Taguchi design of experiments. These experiments are defined by the unique combination of the settings denoted in Table II. This table denotes the collection of parameters tested, their available ranges and the values used in this study. The limitations given for each parameter for the range possible are mostly determined by hardware limitations as defined within the software. The lower boundary of the temperature, however, is arbitrarily defined at a point at which below it is believed that the PLA will not be heated enough to extrude properly. Each run has a high or low setting for each printer process parameter under question, with the different combinations giving a broad spectrum of testing conditions with which the effect of each setting on mechanical properties and loading response can be thoroughly assessed and ranked in importance. The high and low values were based on average slicer settings used for these types of printers, as defined by the manufacturer, with a deviation from

the "normal settings" defining the high and low values. For the layer thickness, for example, the standard setting is designated as 0.2 mm, so a deviation of ±0.1 mm was made to determine the high and low values. The printer manufacturer recommends an extrusion temperature of 230°C for all prints, with temperatures higher than this being likely to cause warping of the component. As such, 230°C was chosen as the upper boundary for temperature and 215°C was chosen as the lower, as this is approximately a 5 per cent difference from the recommended setting which can accurately be achieved by the extruder. The difference between the infill directions of 90/180° (aligned) and 45/135° (biased) is shown in Figure 1. The 90/180° orientation is the standard produced by the printer, where the extruded strands are aligned with the axes of the print plate, while the biased 45/135° infill direction is the same internal structure but rotated to produce a 45° diagonal version of the aligned structure. Using these two configurations gives two very distinct sets of microstructures, which should lead to differences in failure modes between similar runs.

By typical FFE calculation, the experimental array necessary to thoroughly assess the effect of each setting on material properties leads to 2^6 unique experiments; however, with testing for both tensile and fracture properties, the number of experiments doubles. Due to the nature of FDM printing, there exist three orientations in which samples may be printed, as shown in Figure 2. This diagram shows both tensile and fracture coupons in the three types of manufacturing orientations possible with this FDM device. Additionally, to detect and mitigate the effects of outliers, three samples were tested for each experiment at each orientation. Summing up the total number of tests needed by the FFE format under the given conditions, this leads to a total of 1,152 necessary test specimens.

Using the Taguchi method, however, the experimental array is calculated as an orthogonal L8 array, leading to eight

Figure 1 Visualization of low (90/180°) and high (45/135°) value settings for the infill direction process parameter
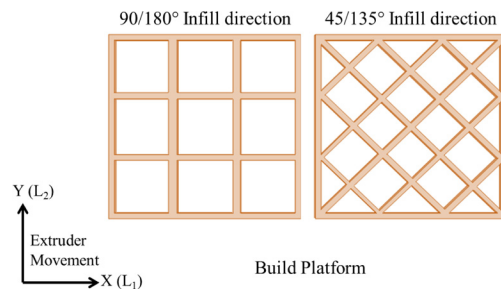
Table II Processing parameters used with range of values possible, minimum increments possible and actual values used during testing given

Processing parameter	Range possible	Minimum increment	Settings used (low/high)
Temperature (°C)	T_m-280	1	215/230
Speed (mm/s)	10-200	1	60/120
Infill direction (°)	0-180	N/A	0/90 and 45/135
Relative density/infill (%)	0-100	1	35/100
Layer thickness (mm)	0.10-0.40	0.05	0.1/0.3
Perimeter	Off/On	N/A	Off/On

Figure 2 Naming convention for the FDM fracture and tensile specimens

Figure 3 Specimen designs and dimensions for (a) fracture testing following ASTM D5405 and (b) tensile testing following ASTM D638 guidelines
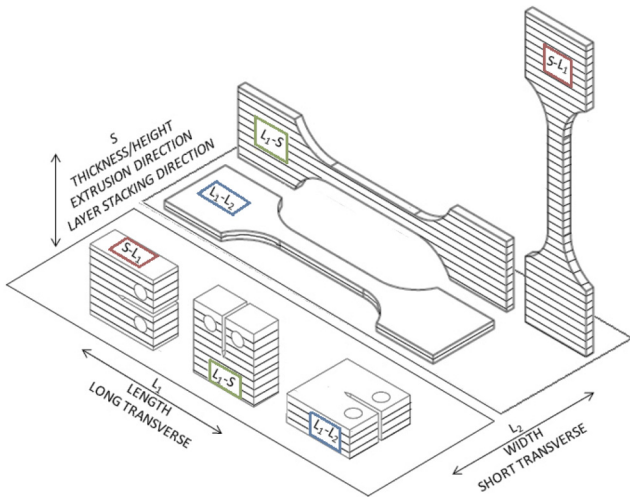
ensembles of experiments, or runs, necessary for analysis of the six variables chosen, as shown in Table III. Each run is an experiment with a specific combination of high/low values for each setting, as denoted by the requirements of the L8 array. With three orientations being tested with three samples for each orientation for both fracture and tensile experiments, the total number of specimens required to be tested becomes 144, an eighth of the 1,152 test specimens required by the FFE.

Tensile and fracture testing specimens were prepared according to dimensions specified by ASTM standards D638 and D5045 for tensile and fracture testing of plastics, respectively (ASTM, 2010, 2007). Specimen design and dimensions for both tensile and fracture tests are shown in Figure 3. Tensile testing specimens were manufactured in the dog-bone shape, while fracture tests used the compact tension specimens. The naming convention was derived from ASTM E399, with modifications made according to the layering orientation (ASTM, 2012). Specimens were named by the direction of loading, followed by the direction of expected crack propagation or rupture, as shown in Figure 2. It should be noted, however, that other permutations exist for loading and cracking directions, which were not chosen for this study, as preliminary testing revealed strong similarity to the three chosen, due to the symmetrical nature of how the FDM

machine prints samples. The material behavior can be classified as a special case of orthotropy with S, L_1 and L_2 being primary stress axes. Properties in L1 and L2 (for 90/180°) are expected to be identical, yet the material is not isotropic in the L_1-L_2 plane. The orientations used (along with those which were not used due to equivalence) are: S-L_1 (S-L_2), L_1-S (L_2-S) and L_1-L_2 (L_2-L_1).

The importance of orientation has been thoroughly documented, especially when considering the tensile response of FDM components, as printing the layers such that the direction of tensile loading is along the length of the layers, rather than perpendicular to them, leads to the greatest tensile strength (Ahn *et al.*, 2002; Sood *et al.*, 2010). This is due to the load being applied along the length of the stacked layers, providing the best distribution of loading. Though many of these studies typically concentrate on FDM samples manufactured from ABS thermoplastics, these identical principles apply for other FDM parts from different materials with similar layering. The fracture properties of FDM components have not been exhaustively investigated, especially as they relate to PLA, as the fracture properties of bulk PLA are not very thoroughly documented. It is important

Table III Runs designed via use of Taguchi L8 test matrix

Run	Temperature, T (°C)	Speed, s (mm/s)	Infill direction, θ (°)	Relative density, ρ (%)	Layer thickness, δ (mm)	Perimeter layer, P
1	215	60	90/180	35	0.1	Off
2	215	60	90/180	100	0.3	On
3	215	120	45/135	35	0.1	On
4	215	120	45/135	100	0.3	Off
5	230	60	45/135	35	0.3	Off
6	230	60	45/135	100	0.1	On
7	230	120	90/180	35	0.3	On
8	230	120	90/180	100	0.1	Off

Note: Each of these runs will be tested with three samples at each of the three orientations denoted in the text: L_1-L_2, S-L_1 and L_1-S

Fused deposition modeling with polylactic acid
Ali P. Gordon et al.

Rapid Prototyping Journal
Volume 22 · Number 2 · 2016 · 000–000

to characterize the influence of material orientation on both tensile and fracture properties to determine which orientation will provide the best results for each situation or when a combination or balance of strengths is desired, and also to develop a streamlined optimization process.

During preliminary tests conducted prior to this study, the perimeter, or outer shell, of the object would often display unique behavior different from the infill of the object. Although an object cannot be printed without at least one perimeter layer, the influence of the perimeter layer on mechanical properties should also be explored. As such, for those samples which call for no perimeter layer, the perimeter had to be manually removed, taking care not to damage the internal structure of the components, which could affect results. For those tested with the perimeter layer left attached, the printer was set to add two layers, as is the standard setting for this printer. The thickness of these layers was dictated by the thickness setting; thus, if the layer thickness was set to 0.1 mm, the perimeter layers also printed at 0.1 mm.

Testing procedures followed those set by ASTM standards D638 and D5045 (ASTM, 2010; 2007) in an ambient environment, utilizing an electromechanical universal test machine (MTS 1kN) and TestWorks software; the constant displacement rate was set to 1.524 mm/min (0.001 in/sec) with a data capture frequency of 5 Hz. A direct contact extensometer (MTS model 634.11E-25) was used for extension measurement during tensile testing, as shown in Figure 4, and a MTS (model no. 632.02E-20) clip gauge was used to measure crack tip opening displacement for fracture tests. Due to the flexible nature of thermoplastics, the range of displacements encountered during tests was often beyond the capabilities of the measurement devices used. As such, a simple method was derived to account for the large deflections. For the fracture tests, the clip gauge would be removed just before it would reach its limiter at 5 mm, which would have also ended the test prematurely. A correlation was made between the displacement recorded from the clip gauge

Figure 4 Tensile specimen during testing in MTS electromechanical universal test machine attached via mechanical wedge grips (model #M2 0-250 S25) with direct contact extensometer attached

and that exported by the crosshead; the displacement could then be estimated beyond that which the instrument could measure from this correlated equation using the load-line displacement. The same procedure was conducted for the tensile tests; however, the extensometer was not needed to be removed mid-test. Consequently, a linear calibration was established between extension and clip gauge/extensometer displacement to calculate large sample deflections. The collected data were then analyzed to determine the mechanical properties and how the individual printing processes affect them. The test specimens were analyzed to study the rupture modes, as they relate to printing orientations and the subsequent effects on material properties.

3. Experimental mechanical testing results

3.1 Tensile testing

The results acquired via tensile and fracture tests support the well-documented fact that orientation plays a primary role in the performance of FDM manufactured parts (Ahn *et al.*, 2002; Sood *et al.*, 2010). This applies to all runs conducted, for both fracture and tensile specimens, though the best-performing orientation and run differ for the two specimen types. The extent of this dependence, however, varies from run to run, as shown in Figure 5, which displays the stress–strain response of select tensile runs. Although a general trend can be observed for each specimen type on the reliance of performance on orientation, the difference in strength between different orientations varies between runs due to the variations in print parameter settings. This can be seen when comparing tensile Run 1 [Figure 5(a)] to Run 2 [Figure 5(b)], in which the main differences are relative density, layer thickness and the presence of a perimeter layer. In Run 1, the three stress–strain curves are closely grouped together, but in Run 2, there is a clear difference between the three curves, so the effects of print orientation become evident. The clear trend here is that the L_1-S orientation is the least likely to fail for components which will experience a tensile load. Recalling Figure 2, it could be expected that L_1-S and L_1-L_2 would display similar response behaviors due to the layout of the layers being along the direction of loading, rather than perpendicular to it, such as in S-L_1. The stress–strain curves of the different runs in Figure 5 show that this is not the case. Due to the nature of the printing process, the L_1-S orientation has more load-bearing fibers, meaning that more fibers print parallel to the direction of the load, with very short perpendicular fibers. The L_1-L_2 samples, then, have numerous long fibers which run perpendicular to the load which will delaminate rather than deform, reducing the total number of load-bearing fibers in the structure and significantly reducing strength, as shown in Figure 6. The difference in the load-bearing area is notable when comparing the lighter portions of each sample, as these are areas which deformed before failure, rather than separating by delamination or sudden fracture, as is indicated by the darker, transverse strands of Figure 6(a). Of note in these images is the tendency of the perimeter layers to separate from the bulk of the sample, particularly for L_1-L_2, which decreases load-bearing capabilities. This phenomenon is likely due to the use of the lower temperature setting. Additionally, in Figure 5(b) and (c), a behavior is observed outside of the logically expected

F4

F5

F6

Figure 5 Effects of material orientation and process settings on tensile strength of FDM PLA
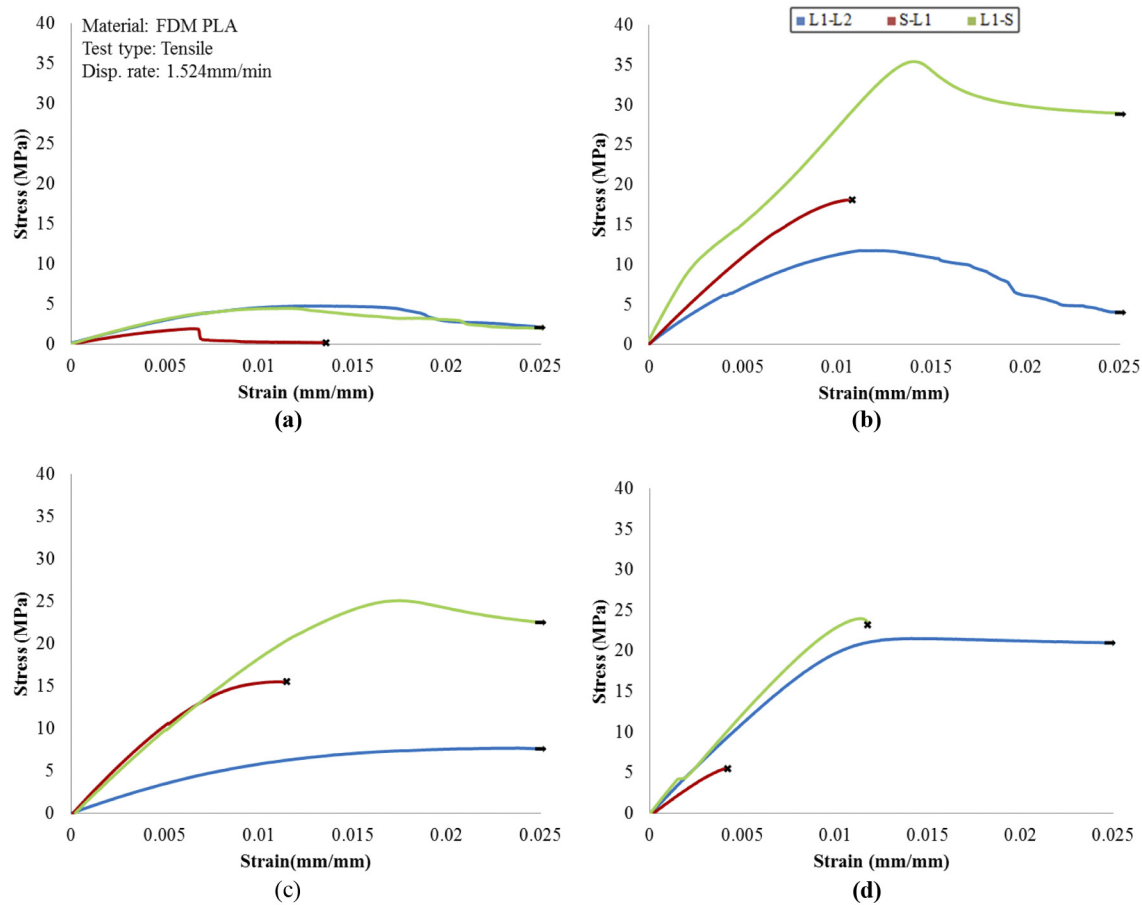
Notes: (a) Run 1: $T = 215°C$, $s = 60$ mm/s, $\theta = 90/180°$, $\rho = 35$ per cent, $\delta = 0.1$ mm, $P = $ On; (b) Run 2: $T = 215°C$, $s = 60$ mm/s, $\theta = 90/180°$, $\rho = 100$ per cent, $\delta = 0.3$ mm, $P = $ On; (c) Run 4: $T = 215°C$, $s = 120$ mm/s, $\theta = 45/135°$, $\rho = 100$ per cent, $\delta = 0.3$ mm, $P = $ Off; (d) Run 6: $T = 230°C$, $s = 60$ mm/s, $\theta = 45/135°$, $\rho = 100$ per cent, $\delta = 0.1$ mm, $P = $ On

outcomes in which the samples built in the $S-L_1$ orientation, which are expected to display the worst tensile response, achieve a higher tensile strength than that achieved in the L_1-L_2 orientation. This is due to the non-uniformity of the rupture mechanism, as shown in Figure 6(a), where it can be seen that separate strands deform independently and to different extents, the resulting fracture varying in levels of deformity and strand length, whereas those of Figure 6(b) deformed uniformly and cohesively, withstanding a larger amount of force before failure. As such, the interlayer bond strength of the $S-L_1$ components shown in Figure 5(b) and (c) exceeds the tensile strength of the corresponding L_1-L_2 components due to the individual strands of the structure deforming non-uniformly from one another, rather than as a single cohesive unit.

Further inspection of Figure 5 shows that tensile Run 1 conferred the weakest mechanical properties of all runs with yield strength of 4.7 MPa, compared to that achieved by Run 2 at 32 MPa as the highest. Runs 4 [Figure 5(c)] and 6 [Figure 5(d)], on the other hand, performed relatively well in comparison to the remaining runs. Comparing the settings between these runs demonstrates that the low ρ and low δ

facilitate weak mechanical properties. This implies that the highest values for tensile properties such as yield strength are closely connected to 100 per cent relative density, ρ, and 0.3 mm layer thickness, δ, settings. Run 4 yielded slightly higher u_t and σ_{uts} values than Run 6, and this is likely attributed to having both a high density and layer thickness, such as in Run 2; these values being lower than that of Run 2 can be attributed to either utilizing the alternate infill direction of 45/135° making the strands less resistant to the tensile load due to their offset orientation or the lack of a perimeter layer. The properties yielded by Run 6 are close to those of Runs 2 and 4, despite the lower 0.1 mm δ, but a higher T of 230°C, as opposed to the lower setting of 215°C for Runs 1-4. From this, it is observed that for tensile samples, the most important settings are high density and high layer thickness. High temperature and the presence of a perimeter layer are also suspect of impacting tensile response from the aforementioned observations. For the L_1-S direction, the presence of a perimeter layer could simply be advantageous, as it provides extra layers to reinforce the structure, and this could be part of the difference in the performances of Runs 2 and 4, such as the yield strengths being 32 and 23 MPa, respectively. Also

Figure 6 Tensile failure mechanisms for (a) L_1-L_2 orientation which displays non-uniform deformation at the rupture site as opposed to (b) L_1-S orientation which shows a nearly uniform fracture surface

(a)

(b)
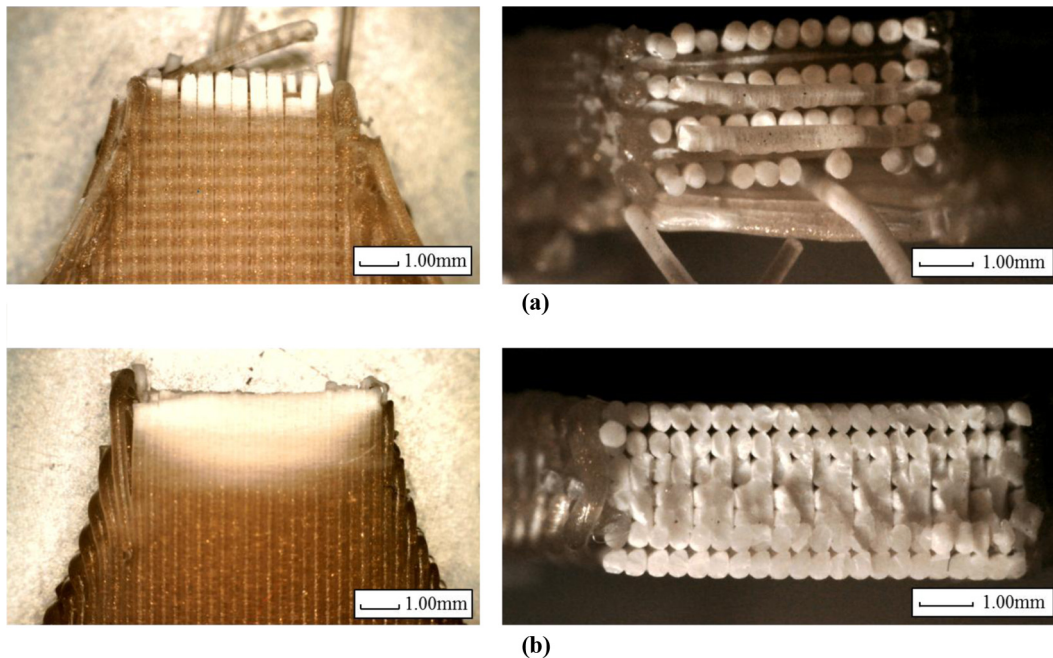
important to note from Figure 5 is that for all three orientations of most runs, the peak stress seems to occur at around 0.01 to 0.015 mm/mm, though it is slightly lower for some of the runs in the S-L_1 orientation, closer to 0.005 mm/mm. This is due to the delamination of layers, as the bond between the layers is weaker than that of the layers themselves, so the sample delaminates rather than deforming.

Examining the individual mechanical properties yielded by each run and comparing them by orientation allow for more thorough analysis. Figure 7 displays the ultimate tensile strength of the samples, σ_{uts}; the yield strength, σ_y; the elastic modulus, E; and the modulus of toughness, u_t. The modulus of toughness is calculated as:

$$u_t = \int_0^{\sigma_{uts}} \varepsilon d\sigma \qquad (2)$$

The toughness was calculated up to the point of σ_{uts} rather than to rupture, as is traditionally done, due to the vast differences in material response between the different orientations and runs beyond this point. As some samples within a run set ruptured at the point of σ_{uts} and some experienced large plastic deformations before rupture, this calculation helps to eliminate some of the behavior discrepancies between samples. This measure is not done to penalize or underestimate samples which may have performed well, rather to eliminate inconsistencies which arise in testing due to the unpredictable deformation behavior beyond the point of σ_{uts}, which is also often the furthest point of usability of a component, and thus the point of greatest interest to most users.

Runs 1 and 3 both have a combination of low T, δ and ρ and display poor tensile properties; this is likely due to the combination of low density and thickness, though the low temperature likely reduces their performance further. Inspection of Run 2 in the L_1-S orientation, which clearly outperforms all other run/orientation combinations in terms of load support with yield strength of 32 MPa, combined with the aforementioned observation leads to the conclusion that both high density and layer thickness are required for good tensile response. Runs 6 and 7, with similar though slightly lower yield strengths of 25 and 26MPa, respectively, and which do not have both high density and layer thickness, rather the combination of either 100 per cent density and 0.1 mm layer thickness (Run 6) or 35 per cent density and 0.3 mm layer thickness (Run 7) plus high temperature (230°C), show that it is important to have both of these settings on high to achieve maximum tensile strength. This is also an indication that high temperature provides a significant strength increase over samples produced at the lower temperature, as successive layers will develop more cohesive properties. Moreover, these results indicate that low performance actually comes from the combination of 35 per cent relative density and the low layer thickness setting of 0.1 mm, as this is what yields poor, low-control print quality such as that seen in the microscopy of the inner structure of samples from Run 1, which bears this combination of attributes, as shown in Figure 8. This microstructure shows uneven thickness and spacing throughout the print, rather than consistent overlapping strands which add strength to the structure.

Although tensile properties favor the settings for Run 2 in the L_1-S orientation, which resulted in the highest values for yield strength and ultimate tensile strength, Runs 4 and 6 resulted in higher E values. This is attributed to one of the samples in each of these run/orientation combinations having a very different response from the other two samples, as shown in Table IV. Run 2 has one sample with a significantly lower response than the other two samples, which are much closer

Figure 7 Comparison of tensile properties across all tensile test runs
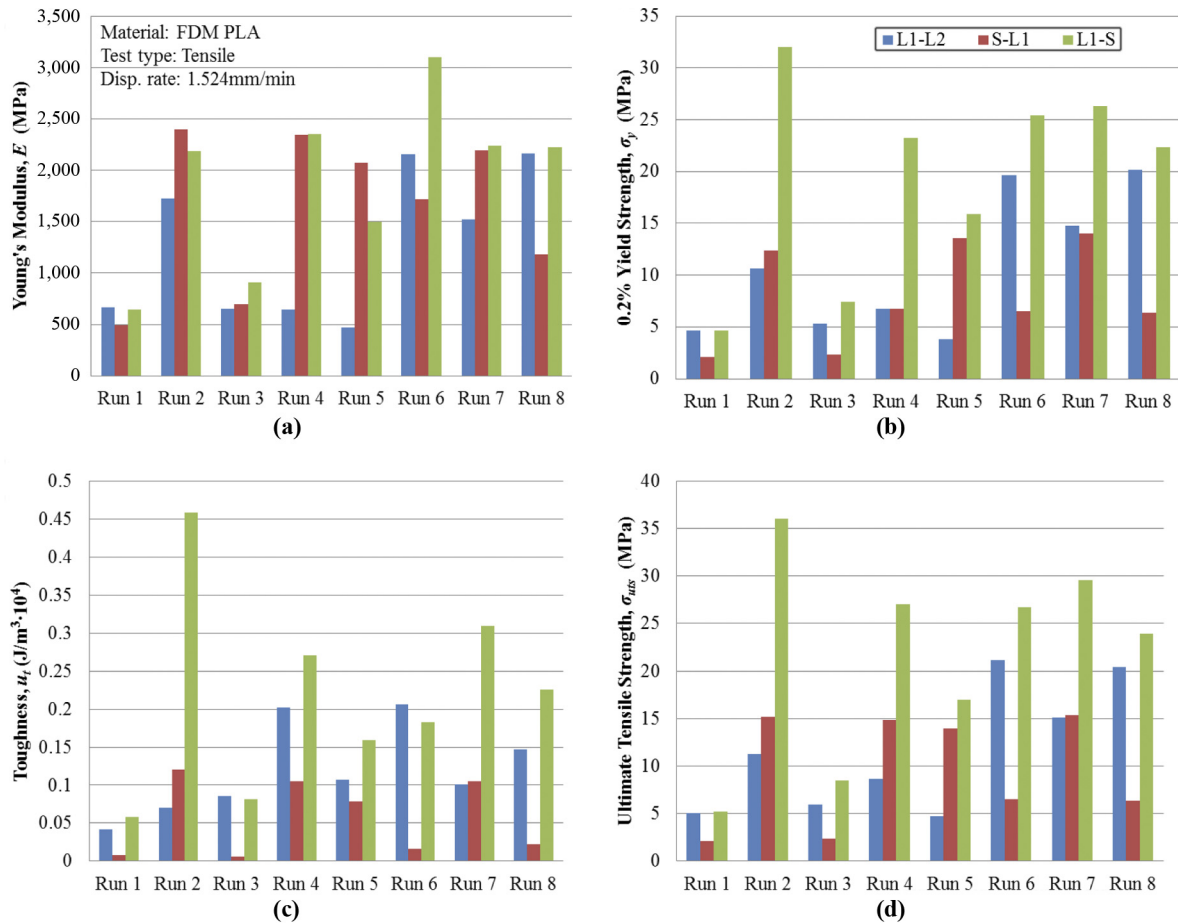
Notes: (a) Elastic modulus, E; (b) 0.2 per cent yield strength, σ_y; (c) modulus of toughness, t_t; (d) ultimate tensile strength, σ_{uts}

together, reducing the average. Runs 4 and 6, on the other hand, both have one sample with a significantly higher response. Although all three samples from Run 6 have a very varied response, Sample 1 is much higher than the other two, this being considered the outlier. The existence of these outliers is considered to be responsible for the variation in responses from the trend which exists for all other properties. Likely, having a larger number of samples would place the values for these much closer together, eliminating the large levels of statistical variance. Omitting these outliers results in average values which are much closer together than those calculated using all three samples, though Run 6 still has the highest value, likely due to the use of a higher temperature.

3.2 Fracture testing

The dependence of performance on orientation is as evident in the fracture testing results, as it was in the tensile testing results. Figure 9 shows the load versus displacement behavior of the fracture samples for the same four runs as displayed for the tensile samples for a direct comparison. This time, however, the L_1-L_2 orientation is clearly the best-performing orientation in terms of mechanical properties related to the fracture tests, as opposed to the L_1-S orientation, which

outperformed the others in the tensile tests. This is due to the nature of the fracture test and the sample orientation. Due to the material orientation, when the test is conducted, the crack must propagate through multiple layers at once, rather than one layer at a time, as would be the case for the L_1-S samples. As the crack tip advances in the L_1-L_2 samples, it encounters multiple continuous layers throughout the entire sample, as opposed to having to tear through a single layer at a time in the L_1-S samples, which may lead to delamination of the printed layers once the crack completely severs through one of the layers. This can be seen in Figure 9(c), where the sample undergoes out of plane cracking because the energy needed to transversely rupture fibers at the crack tip is too great. The L_1-S sample depicted delaminates at the mounting points of the sample after tearing through only a few layers, rather than tearing through the entire structure, as the L_1-L_2 sample does. Although failure occurs in the expected direction for the S-L_1 sample, Figure 9(b), inspection of the fracture surface reveals that this sample also delaminates, this time along the thinnest part of the component at the tip of the crack.

Fracture behavior and the effects of production variables can be determined by examining both the load-displacement response of each of the runs as well as the resulting mechanical

Figure 8 Microstructure of low-density, low-thickness sample from Run 1
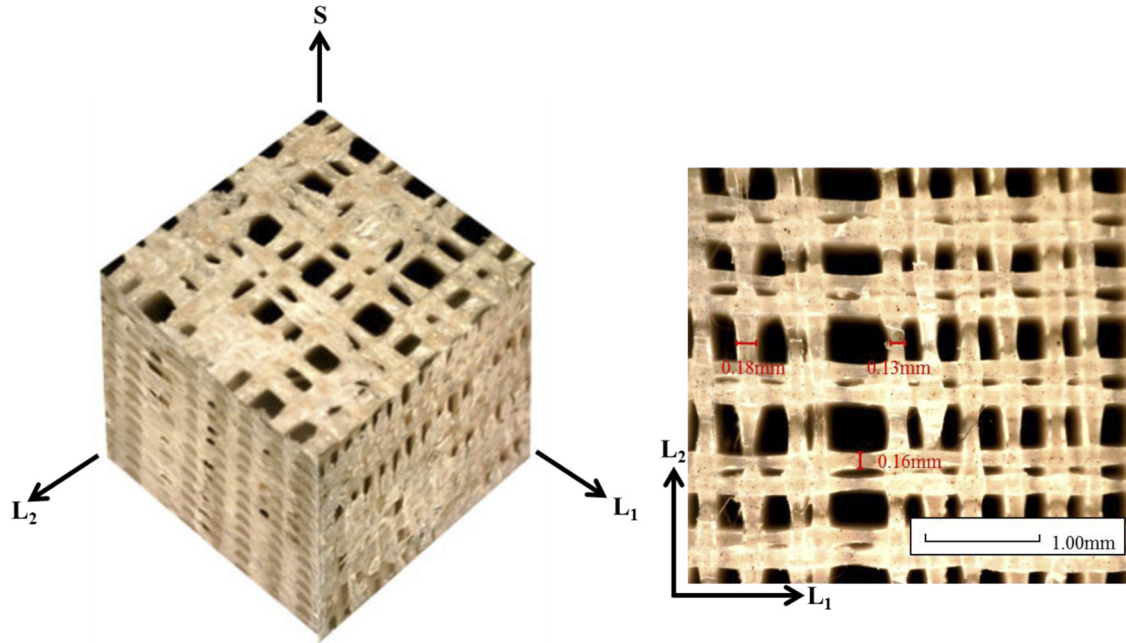
Notes: $T = 215°C$; $s = 60$ mm/s; $\theta = 90/180$; $\rho = 35$ per cent; $\delta = 0.1$ mm; $P = $ off

Table IV Calculation of elastic modulus for all tensile samples printed in the L_1-S orientation for Runs 2,4 and 6 highlighting outliers and noting their effects on the average values for each run

Run no.	Sample 1 (GPa)	Sample 2 (GPa)	Sample 3 (GPa)	Average w/ outlier (GPa)	Average w/o outlier (GPa)
Run 2 ($T = 215°C$, $s = 60$ mm/s, $\theta = 90/180°$, $\rho = 100\%$, $\delta = 0.3$ mm, $P = $ On)	2.42	2.63	**1.51**	2.19	2.53
Run 4 ($T = 215°C$, $s = 120$ mm/s, $\theta = 45/135°$, $\rho = 100\%$, $\delta = 0.3$ mm, $P = $ Off)	**2.82**	2.10	2.15	2.36	2.12
Run 6 ($T = 230°C$, $s = 60$ mm/s, $\theta = 45/135°$, $\rho = 100\%$, $\delta = 0.1$ mm, $P = $ On)	**3.89**	2.86	2.56	3.10	2.71

properties. Examining the curves in Figure 9(d) reveals that Run 6 yields the highest fracture response and as was the case in the stress–strain curves from the tensile experiment; Run 1 yields the least load support, failing at significantly lower load levels than other runs. This can be further corroborated by inspection of the individual mechanical properties yielded by each run compared by orientation in Figure 10. This figure shows the critical stress intensity factor, K_Q; the ultimate load, P_{ult}; the fracture energy, U_{TF}; and the strength ratio, R_{sc}. The critical stress intensity factor was calculated according to (ASTM, 2012):

$$K_Q = \frac{P_Q}{B\sqrt{W}} \, f\left(\frac{a}{W}\right) \quad (3)$$

where B is the specimen thickness, W is the specimen width, a is the initial crack length and:

$$f\left(\frac{a}{W}\right) = \frac{\left(2 + \frac{a}{W}\right)\left(4.65 \frac{a}{W} - 13.32 \frac{a^2}{W^2} + 14.72 \frac{a^3}{W^3} - 5.6 \frac{a^4}{W^4}\right)}{\left(1 - \frac{a}{W}\right)^{\frac{3}{2}}} \quad (4)$$

The requirement for the stress intensity factor, K_Q, to be used as the fracture toughness, K_I, for the material is:

$$B, a \geq 2.5 \left(\frac{K_Q}{\sigma_y}\right)^2 \quad (5)$$

This requirement is met by all configurations except Run 4 of the L_1-L_2 orientation. An additional requirement is that the ratio of P_{ult}/P_Q does not exceed 1.10 for K_I to be valid. All runs from the L_1-L_2 orientation do not meet this requirement; thus, the strength ratio, R_{sc}, is calculated according to (ASTM, 2012):

$$R_{sc} = \frac{2P_{max}(2W + a)}{B(W - a)^2 \sigma_y} \quad (6)$$

Here, the strength ratio is a unitless description of material toughness. The combination of settings for Run 4 ($T = 215°C$, $s = 120$mm/s, $\theta = 45/135°$, $\rho = 100$ per cent, $\delta = 0.3$ mm, $P = $ Off) seems to yield the highest toughness when calculated in this manner; however, using samples of the same size, K_I was calculated as if all of these validity factors were

Figure 9 Effects of material orientation and process settings on fracture strength of FDM PLA
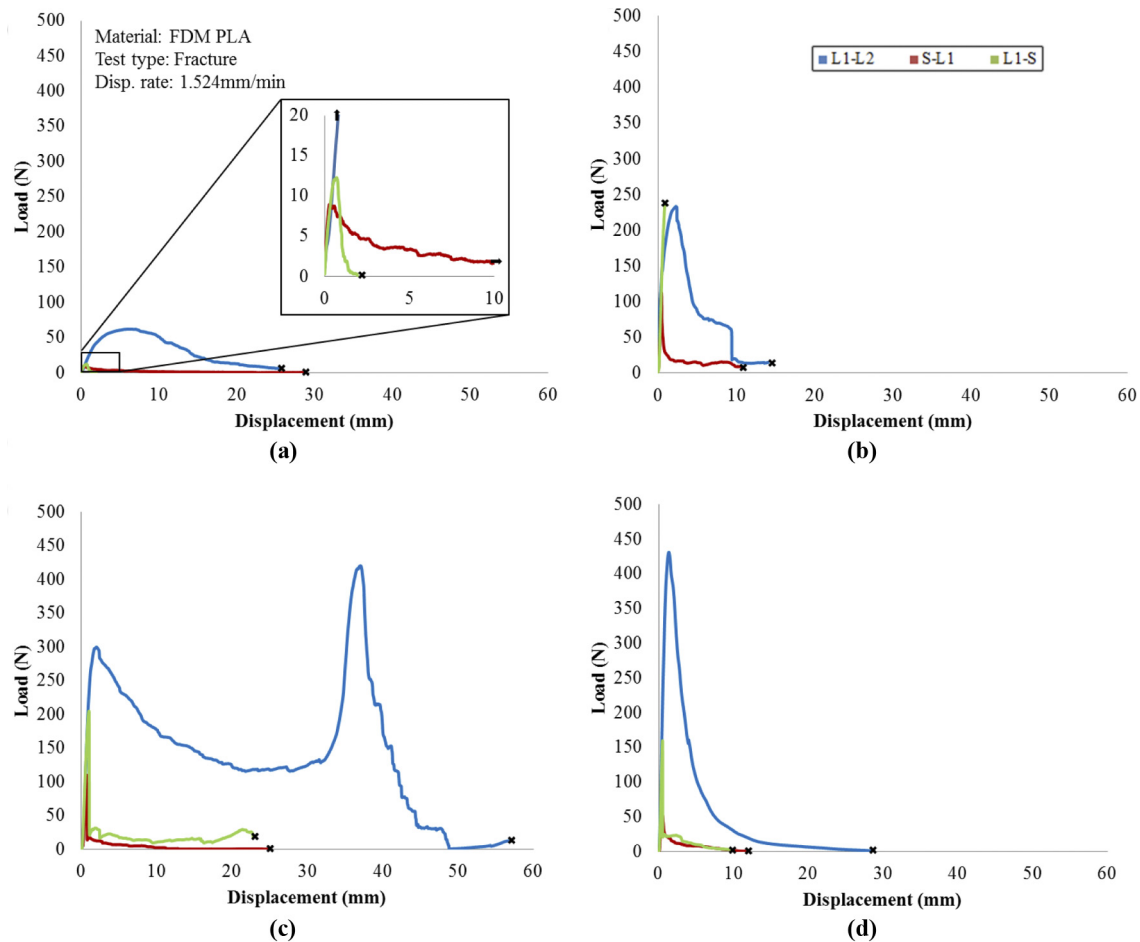
Notes: (a) Run 1: $T = 215°C$, $s = 60$ mm/s, $\theta = 90/180°$, $\rho = 35$ per cent, $\delta = 0.1$ mm, $P = $ On; (b) Run 2: $T = 215°C$, $s = 60$ mm/s, $\theta = 90/180°$, $\rho = 100$ per cent, $\delta = 0.3$ mm, $P = $ On; (c) Run 4: $T = 215°C$, $s = 120$ mm/s, $\theta = 45/135°$, $\rho = 100$ per cent, $\delta = 0.3$ mm, $P = $ Off; (d) Run 6: $T = 230°C$, $s = 60$ mm/s, $\theta = 45/135°$, $\rho = 100$ per cent, $\delta = 0.1$ mm, $P = $ On

met. These K_I values should not be cited as direct figures of correctly calculated fracture toughness, as only some of the runs met the aforementioned conditions. The values calculated serve as a way to assess the general behavior of each sample and the trends or effects which arise from the varying run settings. As such, in this document, the critical stress intensity factor will be primarily discussed, though the toughness may be referred to as well, both cases will refer to the same value of K_Q as calculated above.

Comparing the performance of the individual runs for specific fracture properties, namely, maximum load and critical stress intensity factor, further supports the observation that Run 6 ($T = 230°C$, $s = 60$ mm/s, $\theta = 45/135°$, $\rho = 100$ per cent, $\delta = 0.1$ mm, $P = $ On) had the highest performance. However, the graphs in Figure 10 also reveal that the Run 8 settings achieved comparable results in terms of these properties. This likeness is associated with the high density (100 per cent) and low layer thickness (0.1 mm) prints, which develop numerous thin layers across the crack tip which must be simultaneously broken to facilitate brittle fracture. Any one of these thin layers could also contribute to out-of-plane crack

path deflection, further strengthening the structure. The difference between the two, although slight, is attributed to either the presence of a perimeter layer for Run 6, which adds additional bulk and crack resistance to the samples, or to a difference in infill direction, θ, as the 45/135° orientation of layers provides more divisions or gaps throughout the layers which the growing crack will encounter. These very small gaps between filaments act as grain boundaries or lattice imperfections do within a crystalline material, deflecting crack growth and requiring more energy for crack propagation. Additionally, the strands printed in the 90/180° configuration are either parallel or perpendicular to the crack tip, offering less resistance than samples with the 45/135° orientation which are at an angle to the crack tip, causing it to deflect the growth of its direction each time it encounters a strand at a different angle, as displayed in Figure 11. The difference in crack growth shows that the direction of the strands works to divert the crack, not allowing it to grow directly in the expected direction, as it does when using the 90/180° setting, but forcing it to grow diagonally.

F11

Figure 10 Comparison of fracture properties across all fracture test runs
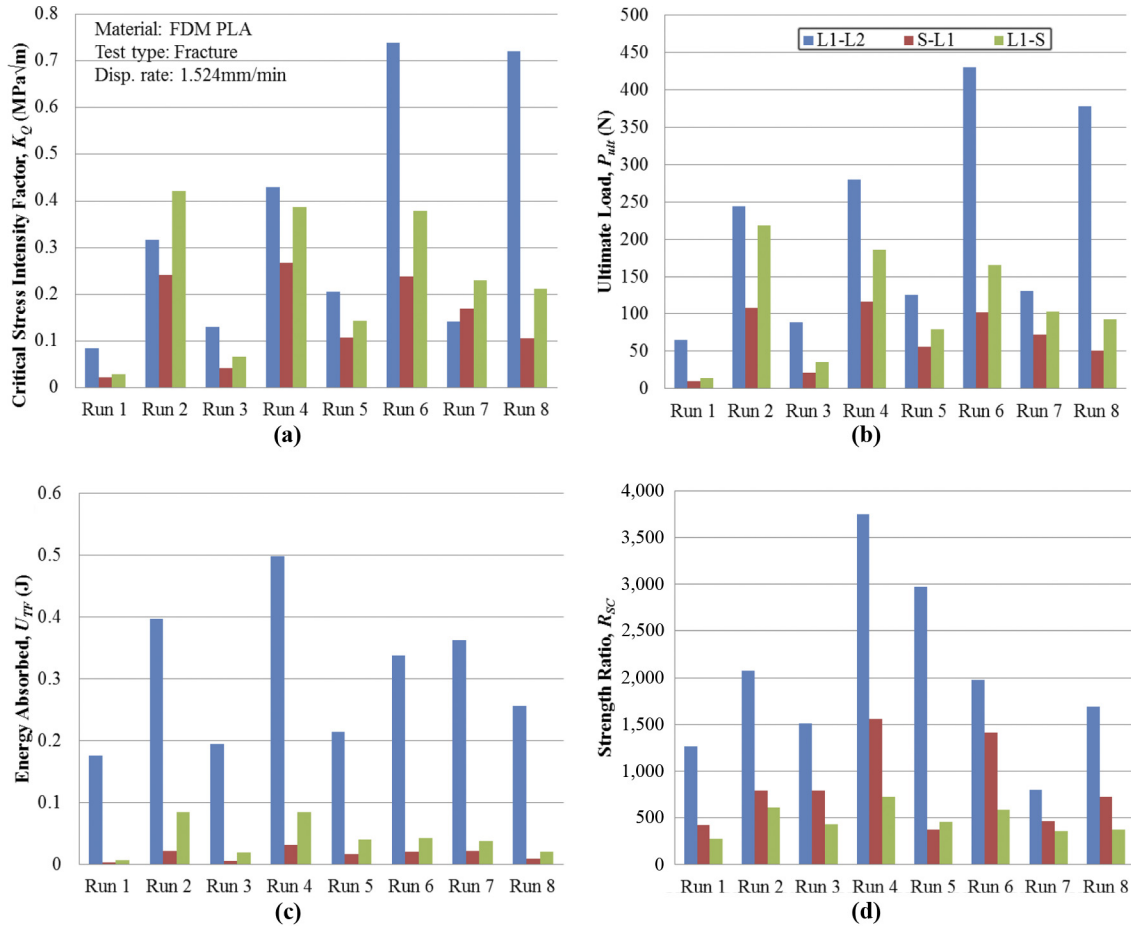
Notes: (a) Critical stress intensity factor, K_Q; (b) ultimate load, P_{ult}; (c) fracture energy absorbed, U_{TF}; (d) strength ratio, RSC

Figure 11 Fracture samples printed in the L_1-L_2 orientation showing crack propagation following infill direction of 45/135° (top row), with the angles of initial fracture denoted, and 90/180° (bottom row)
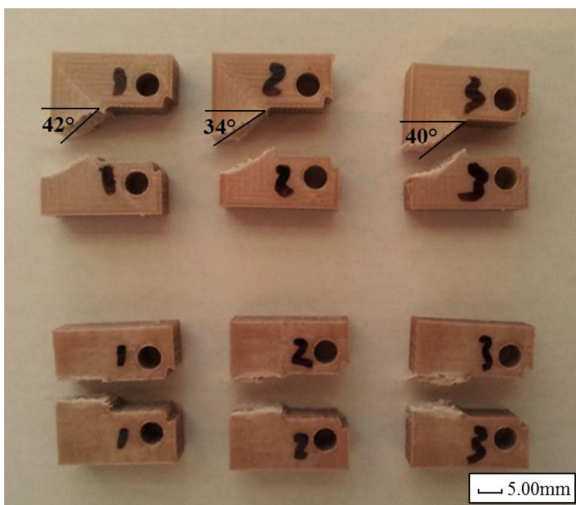
3.3 Discussion

As the previous two sections suggest, there are various points which can be discerned from the individual tensile and fracture results to suggest ways to strengthen samples for either situation. Some key observations can also be made regarding what attributes will weaken PLA FDM structures in general, regardless of orientation or loading mode the structure is expected to endure. Although within each run there is typically a clear difference between orientations, the combinations of 0.1 mm layer thickness and 35 per cent relative density, of Runs 1 and 3, are consistently low performers regardless of which property is being examined or which orientation is being tested. Although there is still some deviation between orientations, it is not nearly as pronounced as in the other runs. This was attributed to the combination of low layer thickness and low infill density, as it is the major commonality between Run 1 and Run 3 which differentiates them from the other runs. Logically, this would be due to the low level of infill, creating a largely porous structure with lots of divisions or faults due to the low layer thickness increasing the number of layers. While this still applies, inspecting the microstructure of the samples reveals that the combination of low density and low layer thickness creates numerous flaws

within the material microstructural fiber patterns. The very thin strands that the extruder is attempting to weave together are poorly controlled at such a small layer thickness and diameter with large gaps in between each strand. The result is illustrated in Figure 8, which shows the microstructure of samples with 35 per cent relative density and 0.1 mm layer thickness (Run 1), as compared to those in Figure 12, which have 100 per cent density and 0.3 mm layer thickness (Run 2). The Run 1 samples with low ρ and low δ, as has been previously noted, have very disorganized, unevenly spaced strands, leading to numerous flaws within the structure. Comparatively, the samples which have 100 per cent infill (from Run 2) have an extremely well-organized and evenly spaced pattern of fibers, with everything cohesively aligned and co-supporting. When the strands are unaligned (Run 1), sagging can occur, as there is minimal support for each strand, further causing distortions within the fiber lattice. All of these flaws will contribute to further weaken the samples, mostly negating the advantage a specific orientation may have in each experiment.

4. Analysis of variance

Further analysis of findings and results based on ANOVA F scores calculated using algorithms embedded into workbooks which utilize equation (1) facilitates ranking the influence level of each setting on each property over all runs. Tables V-VII show the influence of each parameter on each mechanical property for L_1-S, L_1-L_2 and S-L_1 orientations, respectively. These are ranked in order of influence, with first being most influential and sixth being the least. The symbols $+$, $-$ and 0 have been assigned to denote which value the setting should be set to for optimizing that property; $+$ for high, $-$ for low or 0 for null, meaning that for that particular mechanical property, the process and the resulting property value are insensitive to the setting used for the process variable.

These tables show that regardless of orientation, density is by far the most influential setting, with high density always being better than low density for both tensile and fracture samples. Intuitively, this is attributed simply to the fact that a component under loading which has more material over which to distribute that loading will be more resistant to failure, thus enduring higher loading levels and increasing the values of mechanical properties such as yield strength. Fracture strength will increase due to the same reason, as so much open space within the microstructure of the component means that a crack only needs to travel through a very finite amount of material before the component fails; in this case, only 35 per cent of the space beyond the perimeter layers is actually filled with material and provides fracture resistance.

Figure 12 Microstructure of high-density (100 per cent infill), high-thickness (0.3 mm) sample from Run 2
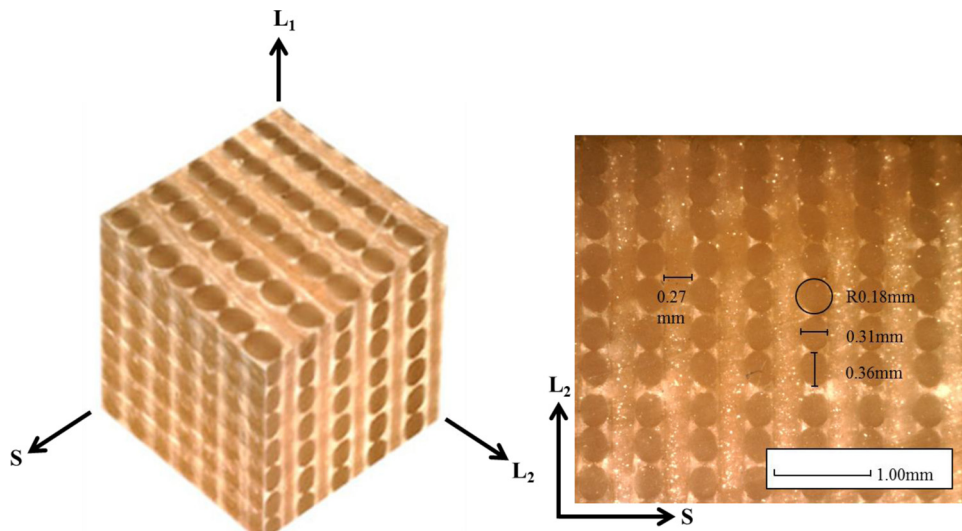
Table V ANOVA ranking of process parameter influence on material properties for L_1-S orientation

L_1-S	Ranking by influence on property					
Material property	1st	2nd	3rd	4th	5th	6th
Young's modulus, E	Density$^+$	Temperature$^+$	Perimeter$^+$	Thickness$^+$	Infill direction$^+$	Speed$^+$
Ultimate tensile strength, σ_{uts}	Density$^+$	Thickness$^+$	Perimeter$^+$	Temperature$^+$	Infill direction$^-$	Speed^0
0.2 % Yield strength, σ_y	Density$^+$	Thickness$^+$	Perimeter$^+$	Temperature$^+$	Infill direction$^-$	Speed^0
Modulus of toughness, u_t	Thickness$^+$	Density$^+$	Infill direction^{--}	Perimeter$^+$	Speed$^+$	Temperature$^+$
Ultimate load, P_{ult}	Density$^+$	Thickness$^+$	Perimeter$^+$	Speed$^-$	Infill direction^0	Temperature^0
Fracture energy, U_{TF}	Thickness$^+$	Density$^+$	Temperature$^-$	Infill direction$^+$	Perimeter$^+$	Speed$^-$
Crit. stress intensity factor, K_Q	Density$^+$	Thickness$^+$	Perimeter$^+$	Speed$^-$	Temperature^0	Infill direction^0

Notes: $+$ for high, $-$ for low or 0 for null

Table VI ANOVA ranking of process parameter influence on material properties for L_1-L_2 orientation

L1-L2	Ranking by influence on property					
Material property	1st	2nd	3rd	4th	5th	6th
Young's modulus, E	Density$^+$	Temperature$^+$	Infill direction $^-$	Perimeter$^+$	Thickness $^-$	Speed^0
Ultimate tensile strength, σ_{uts}	Thickness $^-$	Infill direction $^-$	Density$^+$	Temperature$^+$	Speed $^-$	Perimeter^0
0.2% Yield strength, σ_y	Temperature$^+$	Density$^+$	Perimeter$^+$	Infill direction $^-$	Thickness $^-$	Speed$^+$
Modulus of toughness, u_t	Density$^+$	Infill direction$^+$	Temperature$^+$	Speed$^+$	Perimeter $^-$	Thickness^0
Ultimate load, P_{ult}	Density$^+$	Temperature$^+$	Thickness $^-$	Infill direction$^+$	Perimeter$^+$	Speed^0
Fracture energy, U_{TF}	Density$^+$	Thickness$^+$	Speed$^+$	Temperature^0	Perimeter^0	Infill direction^0
Crit. stress intensity factor, K_Q	Density$^+$	Temperature$^+$	Thickness $^-$	Infill direction$^+$	Perimeter $^-$	Speed$^+$

Notes: + for high, − for low or 0 for null

Table VII ANOVA ranking of process parameter influence on material properties for S-L_1 orientation

S-L1	Ranking by influence on property					
Material property	1st	2nd	3rd	4th	5th	6th
Young's modulus, E	Thickness$^+$	Density$^+$	Temperature$^+$	Perimeter$^+$	Infill direction$^+$	Speed $^-$
Ultimate Tensile strength, σ_{uts}	Thickness$^+$	Density$^+$	Temperature$^+$	Perimeter$^+$	Speed^0	Infill direction^0
0.2% Yield strength, σ_y	Thickness$^+$	Temperature$^+$	Density$^+$	Speed$^+$	Infill direction^0	Perimeter^0
Modulus of toughness, u	Thickness$^+$	Density$^+$	Infill direction $^-$	Perimeter$^+$	Temperature $^-$	Speed$^+$
Ultimate load, P_{ult}	Density$^+$	Thickness$^+$	Perimeter$^+$	Infill direction$^+$	Temperature$^+$	Speed^0
Fracture energy, U_{TF}	Thickness$^+$	Density$^+$	Infill direction$^+$	Perimeter^0	Speed^0	Temperature^0
Crit. stress intensity factor, K_Q	Density$^+$	Thickness$^+$	Perimeter$^+$	Infill direction$^+$	Temperature$^+$	Speed $^-$

Notes: + for high, − for low or 0 for null

Layer thickness comes in at second most influential setting, with the high value being favored for the L_1-S and S-L_1 orientations. However, inspection of the properties in Table VI for L_1-L_2, which is the favored orientation for fracture samples, reveals that low layer thickness is preferential, corroborating the findings deciphered from Figures 9 and 13. Therefore, it can firmly be said that the lower layer thickness which produces a larger number of layers is favorable for crack resistance, raising fracture toughness or critical stress intensity factor, and the higher layer thickness which produces larger layers with less faults results in higher tensile strength. Another interesting fact to consider is that the lower layer thickness setting produces much smaller gaps between the strands of PLA than the higher layer thickness, as shown in Figure 14, which shows the structure of a Run 8 sample with 100 per cent relative density and 0.1 mm layer thickness. This means that more of the area that the crack must travel is filled in but still has plenty of gaps to divert or stall crack growth, resulting in higher fracture toughness. Comparing the microstructures of fracture samples from Run 2 and Run 8 in Figures 12 and 14, both of which have full density but with a 0.2 mm difference in layer thickness, shows that the structure within the component changes significantly as the layer thickness is varied. The sample with the higher layer thickness (Run 2) has symmetrical, even spacing on both sides of the individual strands, while the lower layer thickness sample (Run 8) only has gaps on the right side of the strands, so that not only reduces the amounts of gaps but also fuses the two directions of strands together more continuously. Thus, while the thicker layers of the Run 2 sample with a layer thickness of 0.3 mm produce stronger strands which support a higher tensile load, the thinner 0.1 mm layers seem to result in less overall porosity within the structure and more continuously bonded layers, as the heat retention in this structure should be higher than in the thicker 0.3 mm layer structure due to the reduced air flow within the structure due to decreased gap size. This, with the existence of regularly occurring small gaps to divert crack growth, in turn raises the critical stress intensity factor of the samples with 0.1 mm layer thickness as compared to the 0.3-mm-thick layers.

Temperature seems to be the third most important factor; in cases when infill density and layer thickness are not both identified as the two most influential factors, it is typically because temperature is taking one of these two spots, with the high value nearly always favored. This is likely due to the fact that the 230°C setting of the extruder puts the PLA at a temperature close to but below its melting point, which has been reported to be between 130 and 230°C, depending on various structural properties of the material and its overall composition (Henton *et al.*, 2005). This puts the extruded PLA in a semi-molten state, which improves malleability and adhesion to previous layers, as opposed to the lower 215°C setting. This setting, although still allowing printing, causes the extruded PLA to adhere less to previously printed layers, so that each subsequent layer is still stacked on top of the previous layer, but with minimal bonding, thereby decreasing component strength. It is evident, however, that although the extruder head temperature is set to 230°C, the PLA itself is being extruded somewhere below that temperature, and the temperature that it is actually at will vary given the differences in printer design and heating properties. It can be concluded then, that the ideal temperature setting for printing should be at or around the melting point of the media being used, as this should place it at a temporarily semi-molten state which will improve printability and component strength. Thus, this setting may have to be altered for each specific printer type

Figure 13 Fracture mechanisms of select samples in the (a) L_1-L_2 orientation, (b) S-L_1 orientation and (c) L_1-S orientation

(a)

(b)

(c)
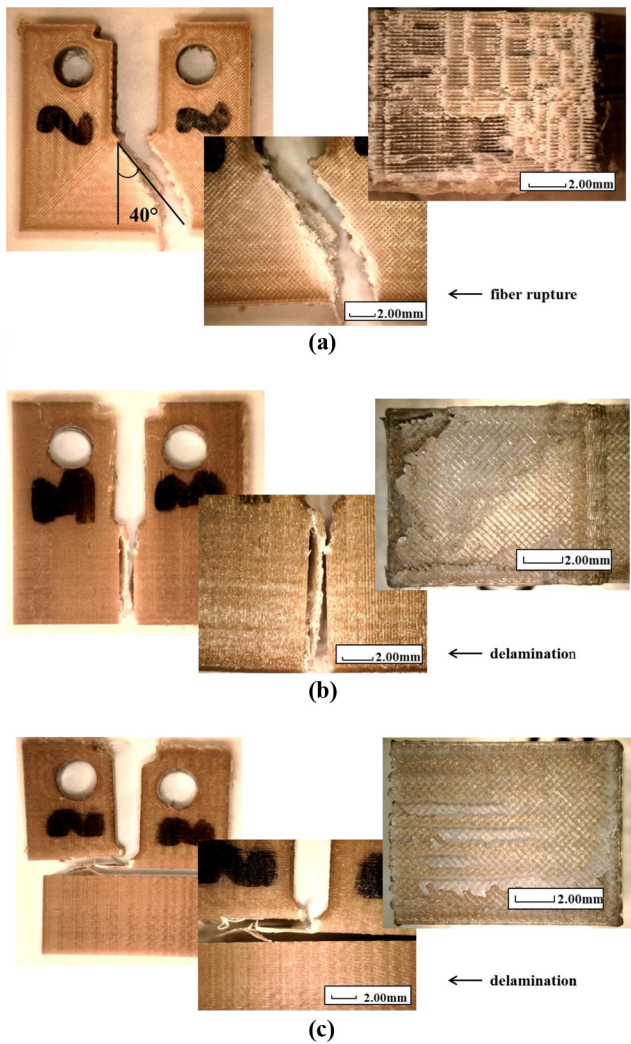
depending on design and the heat properties of both the materials used in the construction of the printer and the printing media. Although the 230°C setting could be said to be a good set point for most FDM PLA printers, the dependency of this setting on printer models may dictate some manipulation of the setting up or down. Though the trend for near-melting point operating temperature still stands, there will be instances where printers with high heat transfer capabilities will cause the PLA to be heated excessively past the semi-molten state and enter a molten state which will prevent it from forming correctly or clog the extruder. The heat retention properties of PLA may also cause warping in the structure in this case, thus endangering both physical and aesthetic properties of the printed component.

Perimeter ranks at the fourth most influential processing parameter, closely following temperature. As may be deduced intuitively, perimeter is better on than off, given that the extra, fully dense layers will add strength regardless of the other setting values. As mentioned in the experimental section, this is not actually a setting that can be turned off as of now, but this setting was tested to gauge the effects of the perimeter layer and how high of an influence it is. It is especially relevant in the L_1-S orientation, ranking at third place for all but one of the material properties. It is of varying importance in the other two orientations, though overall it comes in at fourth and nearly always favors the "on" setting. The most important deduction that can be made here, however, is that if a user wants to use a very low density or infill setting so as to save materials, they could increase the number of perimeter layers to increase the overall strength of the component. The perimeter layer will also affect the way the component fractures, as the perimeter layers do not follow the direction of the infill, rather continuously wrap around the contour of the component, which would increase its strength and resistance to fracture regardless of the direction of loading. This will also vary depending on the number of perimeter layers, with more layers contributing a greater effect. It is important to note that comparison of the response curves of individual samples within a run set for those which underwent manual removal of the perimeter layers (Runs 1, 4, 5 and 8) does not show

Figure 14 Microstructure of high-density (100 per cent infill), low-thickness (0.1 mm) sample from Run 8
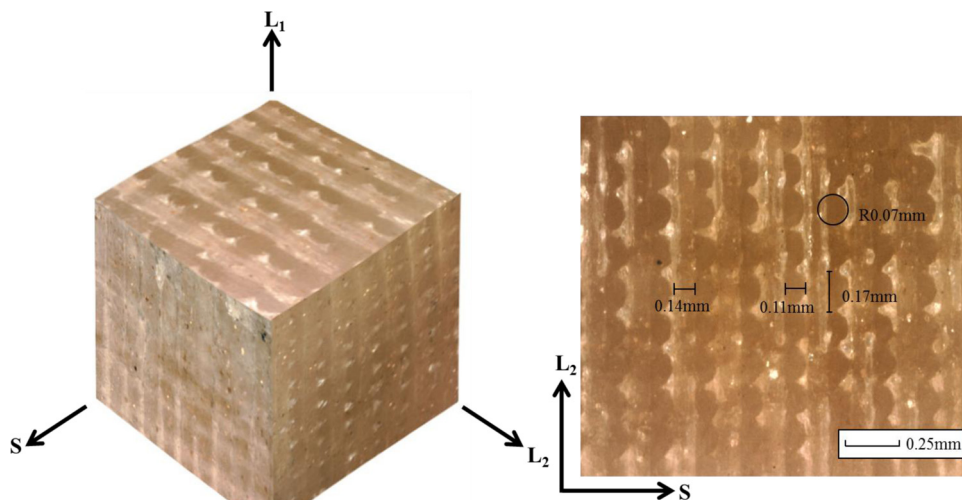
any abnormal behavior beyond that which is expected or shown by samples which were unaltered. This is due to the careful removal of the perimeter layers while preserving microstructural integrity during sample preparation to verify the effects of the presence of the perimeter layers.

According to the ANOVA tables, speed and infill direction do not seem to affect the mechanical properties much regardless of orientation. The distribution of which value is favored for speed varies almost evenly across the orientations, though it is mostly ranked rather low when compared to other printer parameters, which means which value is chosen will have little or no effect on end results. As the overall majority of the rankings indicate a null or high value, however, the recommendation can be made to use the high value for most situations, in the interest of economizing time, especially when making full-density prints. This will alleviate some of the time added by using the high-density setting. However, speed may also be important for aesthetic factors, as a slower speed will boost surface quality, as it is connected to a higher resolution, though this is at the sacrifice of time. The decision to raise or lower speed should be made by the user based on their rating of importance for surface quality. Of note, the fact that the highest majority of properties in the ANOVA table favored a null value suggests that a value in between the two speeds tested is best for general-purpose use. Given the speeds tested of 60 mm/s and 120 mm/s, this suggests that 90 mm/s would yield favorable results across all situations.

As stated previously, it is intuitive that infill direction affects fracture behavior, as longitudinal fibers are barriers to crack propagation and deflect crack growth, in much the same manner as grain boundaries and lattice imperfections. It is due to this that the ANOVA tables (Tables V-VII) show that infill direction predominantly favors the high value (45/135°) setting for all fracture properties across all orientations, with the addition of a few null values. For the tensile properties, on the other hand, the S-L_1 orientation shows a null/positive split, the L_1-L_2 orientation shows a slightly higher favor to the low value (90/180°) and the L_1-S orientation shows a split between the low and high values. According to the ANOVA tables, the tensile properties tend to favor the 90/180° configuration overall, indicating that minimally larger values for properties such as yield strength and Young's modulus would result from using this infill direction as opposed to the 45/135° configuration. In a generalized view of this setting across both experiments, however, there is greater favor toward the high value setting, with more occurrences of the null value than the negative value. In application, this means

that the 45/135° setting is the more reliable one to use as a default, though if tensile loading is of significantly greater concern, then the 90/180° may be the better default. Alternately stated, this parameter setting is based on the situation, especially given the large number of null values. This is a low-ranking setting in order of importance, however, so choosing either setting as permanent should have little impact even if the situation could be said to call for the other setting.

Comparing the results of these experiments to the bulk material properties as given in literature shows favorable results. From Table VIII, it can be seen that many of the largest values from the experimental results of the FDM PLA fall within the ranges given for bulk material from the various sources under which they are listed. The maximum values achieved for each mechanical property are recorded against bulk properties along with the run and orientation which yielded that result. The large variations within some of the values quoted in the literature stem from the different methods which exist to produce the polymer chains of PLA from lactic acid, two structures of which are noted below the column for Subhani (2011). The D and L subscripts denote which lactic acid isomer is used in synthesizing the PLA compound, the D and L subscripts being an indicator of the spatial configurations of the atoms in the lactide isomer (Meislich, 2010). It has been shown that the combination of poly(L-lactic acid) and poly(D-lactic acid) enantiomers produces a stereocomplex with increased crystallization and varied material properties, such as a higher T_m, which will vary depending on the ratio of the mixture, thus giving the wide range of material properties of Table VIII (Yamane and Sasai, 2003; Garlotta, 2001). It is important to note that when considering fracture toughness or critical stress intensity factor, only the tests on the L_1-L_2 specimens closely followed linear elastic fracture mechanics conditions as denoted in ASTM standard E399 where crack growth is nominally transverse to the applied load, tearing through the layers. This is why this orientation yields the greatest fracture results, as the other two will delaminate or shear before tearing.

5. Optimization

Some generalizations can be made about which process variables should be used depending on the application emphasis and for a general basis according to the results of the runs tested here. For situations where the component will experience tensile loading and tensile properties are of high

Table VIII Comparison of select bulk properties of PLA as reported by literature versus the maximum values achieved experimentally with FDM manufactured samples

	Mechanical properties of monolithic PLA				As tested		
	Ashby and Johnson (2013)	Henton *et al.* (2005)	Subhani (2011)				
Mechanical property			$P_{(L)}LA$[a]	$P_{(D,L)}LA$[b]	Max value	Run[c]	Orientation
Young's modulus, *E (GPa)*	3.45-3.8	3.31-3.86	2.7-4.1	1-3.5	3.1	6	L_1-S
Yield strength, σ_y (MPa)	48-69	110.3-144.8	15.5-150	27.6-50	32	2	L_1-S
Toughness, K_I (MPa · $\sqrt{m}$)	0.7-1.1	–	–	–	0.738	6	L_1-L_2

Notes: [a] $P_{(L)}LA$ – PLA formed exclusively from l-lactides (Garlotta, 2001); [b] $P_{(D,L)}LA$ – PLA formed from the combination of d- and l-lactides to form a stereocomplex with higher T_m and differing material properties (Garlotta, 2001; Subhani, 2011); [c] properties of Run 2: $T = 215°C$, $s = 60$ mm/s, $\theta = 90/180°$, $\rho = 100\%$, $P = $ On and Run 6: $T = 230°C$, $s = 60$ mm/s, $\theta = 45/135°$, $\rho = 100\%$, $\delta = 0.1$ mm, $P = $ On;

importance, the settings of Run 2 ($T = 215°C$, $s = 60$ mm/s, $\theta = 90/180°$, $\rho = 100$ per cent, $\delta = 0.3$ mm, $P =$ On) in the L_1-S orientation yield the most appropriate approximation of ideal settings. This combination yielded the highest yield stress of 32 MPa and ultimate tensile stress of 36 MPa while also giving a comparatively good critical stress intensity factor of 0.421 MPa$\sqrt{}$m, the third highest result overall and the highest value achieved outside of the L_1-L_2 orientation. This may also be applicable for situations where a generally high-strength component is desired and the possibility of sudden failure by delamination or shearing is not an issue or concern.

When an emphasis on fracture properties is desired with consideration being given to maintaining good tensile properties, Run 6 ($T = 230°C$, $s = 60$ mm/s, $\theta = 45/135°$, $\rho = 100$ per cent, $\delta = 0.1$ mm, $P =$ On) in the L_1-L_2 direction will give the best results, yielding a critical stress intensity factor of 0.721 MPa$\sqrt{}$m. These settings are best for manufacturing a component which is slow to fracture, as warning of failure will be given by evidence of crack propagation. This comes at some sacrifice to tensile properties, as the yield strength was lowered to 20 MPa as compared to the maximum of 32 MPa achieved with the Run 2 settings, and thus is more appropriate for components which will not undergo particularly high tensile loading, but may be best for those that will endure low-level cyclic loading.

Run 4 ($T = 215°C$, $s = 120$ mm/s, $\theta = 45/135°$, $\rho = 100$ per cent, $\delta = 0.3$ mm, $P =$ Off) consistently yields medium to high results for all properties, though this is dependent on the orientation which is best for each particular test. This presents a good combination of default settings for general-purpose use, so long as care is taken to choose the appropriate orientation for the component and its intended use. The main implication is that the optimal direction for each test is the orientation which yields the largest cross-sectional area per printed layer.

Given these generalized results based on the tested run combinations, compounded with the results from the ANOVA, an optimization of settings can be deduced which should yield high performance across all properties for use on a regular basis for manufacturing various components. These settings, as shown in Table IX, may be used for any type of generalized loading, where users are not concerned specifically with tensile or fracture properties, but have some concerns over the general material properties and strengths of the components being manufactured. Although the orientation is

Table IX Optimization of settings of processing parameters based on loading situation

Processing parameter	Loading situation		
	General	Tensile	Fracture
Relative density, ρ	100%	100%	100%
Thickness, δ	0.30 mm	0.30 mm	0.10 mm
Temperature, T	230°C	230°C	230°C
Perimeter, P	On	On	On
Speed, s	90 mm/s	60-90 mm/s	90-120 mm/s
Infill direction, θ	45/135°	90/180°	45/135°
Orientation	L_1-S[a]	L_1-S	L_1-L_2

[a] User-defined

denoted as L_1-S, this will be at the discretion of the designer to define and decide upon, as it will be dependent on the expected loading situation and direction and the chosen priority of which type of failure to design against, tensile or fracture. In denoting this setting as L_1-S, the recommendation is being made to define and design for tensile loading. Also given in this table are a summary of the settings when an emphasis is made on tensile or fracture-specific material properties. As noted previously, these will closely resemble the settings of Runs 2 and 6 for tensile and fracture, respectively, with slight modifications to boost material properties based on the ANOVA table results. These changes include raising the temperature from 215°C to 230°C for the tensile settings and noting that speed is given in ranges for both tensile and fracture due to the results of the ANOVA tables. These showed that although a median speed of 90 mm/s is generally best for all situations, the tensile properties showed a slight favor to the slower 60 mm/s speed and the fracture properties showed that the higher 120 mm/s speed may be used without any negative effects on properties, giving slight favor to that setting, especially when time savings are considered.

6. Conclusions

On the broad scale, a joint characterization–optimization method was developed on the basis of standard methods. The adaptability of the approach to a wider range of materials is evident.

DoE was used to construct a set of experiments by which the effects of FDM printer settings on tensile and fracture properties of components produced via FDM using PLA could be explored. The settings of the printer adjusted were the layer thickness, density or infill percentage, extrusion temperature, speed, infill direction and component orientation. Each of these settings was assigned a high and low level to be tested at to determine their effect and the best level for each one. The orientation was tested by printing samples in the three orientations possible when printing via FDM. Tensile and fracture specimens were manufactured and tested according to ASTM standards D638 and D5045. Test results were then analyzed using ANOVA to determine the influence of each setting.

Through tensile and fracture testing of FDM printed samples, guidelines have been established for FDM printers using PLA print media. The variable settings can, therefore, be prescribed based on application. Recommendations have been made for both tensile and fracture applications, as well as a generalized combination of parameters which can be chosen for generic applications which may not necessarily be constructed for a single loading situation. This combination yields consistent medium to high values for all properties tested in comparison to other situations which may yield higher values for either fracture or tensile properties at some sacrifice to the other.

Though the given settings represent the best overall combination as given by test results and ANOVA influence rankings, some of these could be changed due to user or situational preference. A lower layer thickness and slower speed will result in a higher resolution with an improved surface finish when aesthetics are important. Layer thickness could then be lowered with little concern to decreased strength, as has been

previously shown. If there is a desire to reduce material consumption, relative density could be lowered, perhaps to a medium setting of approximately 70 per cent. Though this would decrease strength, an increase in the number of perimeter layers could be used to reduce the negative effect, decreasing the amount of hollow space. For components which will experience negligible mechanical loading, relative density may be sacrificed to the lower setting, as strength will not be an issue and an increase in perimeter layers could be used to prevent it from being too fragile, so that mishandling the component would not cause damage. Additionally, the temperatures studied here are specific to the model printer utilized, with the low setting pertaining to around 95 per cent of the manufacturer-recommended temperature. Due to its impact on material properties, future studies should take care to analyze the optimal temperature setting of the printer in question in the manner shown here with a wider and more refined temperature range, so as to effectively gauge the effects of changing extrusion temperatures.

The suggested settings for tensile, fracture or general use will allow users of desktop FDM printers to produce components in which they can be confident of their desired performance. A methodology has been suggested which can be used to find the most important processing parameters and their settings to identify which parameters will yield optimal material properties with a minimized mechanical test matrix.

References

Ahn, S.-H., Montero, M., Odell, D., Roundy, S. and Wright, P.K. (2002), "Anisotropic material properties of fused deposition modeling ABS", *Rapid Prototyping Journal*, Vol. 8 No. 4, pp. 248-257.

Ashby, M.F. and Johnson, K. (2013), *Materials and Design: The Art and Science of Material Selection in Product Design*, Butterworth-Heinemann, Oxford, UK.

ASTM (2007), *D5045, 1999, Standard Test Methods for Plane-Strain Fracture Toughness and Strain Energy Release Rate of Plastic Materials*, ASTM International, West Conshohocken, PA.

ASTM (2010), *D638 Standard Test Method for Tensile Properties of Plastics*, ASTM International, West Conshohocken, PA.

ASTM. (2012), *E399-12e3 Standard Test Method for Plane Strain Fracture Toughness of Metallic Materials*, ASTM International, West Conshohocken, PA.

Bártolo, P.J. (2011), *Stereolithography: Materials, Processes and Applications*, Springer, New York, NY.

Bijarimi, M., Ahmad, S. and Rasid, R. (2012), "Mechanical, thermal and morphological properties of PLA/PP melt blends", *International Conference on Agriculture, Chemical and Environmental Sciences*, Dubai, pp. 115-117.

Bogue, R. (2013), "3D printing: the dawn of a new era in manufacturing?", *Assembly Automation*, Vol. 33 No. 4, pp. 307-311.

Clarinval, A. and Halleux, J. (2005), "Classification of biodegradable polymers", in Smith, R. (Ed.), *Biodegradable Polymers for Industrial Applications*, 1st ed., Taylor & Francis, Boca Raton, FL.

Crump, S.S. (1992), "Apparatus and method for creating three-dimensional objects", Google Patents.

Drummer, D., Cifuentes-Cuéllar, S. and Rietzel, D. (2012), "Suitability of PLA/TCP for fused deposition modeling", *Rapid Prototyping Journal*, Vol. 18 No. 6, pp. 500-507.

Garlotta, D. (2001), "A literature review of poly(lactic acid)", *Journal of Polymers and the Environment*, Vol. 9 No. 2, pp. 63-84.

Girden, E.R. (1992), *ANOVA: Repeated Measures*, Sage Publications, Newbury Park, CA.

Henton, D.E., Gruber, P., Lunt, J. and Randall, J. (2005), "Polylactic acid technology", in Mohanty, A., Misra, M. and Drzal, L. (Eds), *Natural Fibers, Biopolymers, and Biocomposites*, Taylor & Francis, Boca Raton, FL.

Hopkinson, N. and Dickens, P. (2001), "Rapid prototyping for direct manufacture", *Rapid Prototyping Journal*, Vol. 7 No. 4, pp. 197-202.

Jacobs, P.F. (1992), *Rapid Prototyping & Manufacturing: Fundamentals of Stereolithography*, Society of Manufacturing Engineers, Dearborn, MI.

Jamshidian, M., Tehrany, E.A., Imran, M., Jacquot, M. and Desobry, S. (2010), "Poly-lactic acid: production, applications, nanocomposites, and release studies", *Comprehensive Reviews in Food Science*, Vol. 9 No. 5, pp. 552-571.

Lee, C., Kim, S., Kim, H. and Ahn, S. (2007), "Measurement of anisotropic compressive strength of rapid prototyping parts", *Journal Materials Processing Technology*, Vols 187/188, pp. 627-630.

Lee, C.-T. and Kuo, H.-C. (2013), "A novel algorithm with orthogonal arrays for the global optimization of design of experiments", *Applied Mathematics & Information Sciences*, Vol. 7 No. 3, pp. 1151-1156.

McMains, S. (2005), "Layered manufacturing technologies", *Communications of the ACM*, Vol. 48 No. 6, pp. 50-56.

Meislich, H. (2010), *Schaum's Outline of Organic Chemistry*, McGraw-Hill, New York, NY.

Mellor, S., Hao, L. and Zhang, D. (2014), "Additive manufacturing: a framework for implementation", *International Journal of Production Economics*, Vol. 149, pp. 194-201.

Miller, R.G. (1997), *Beyond ANOVA: Basics of Applied Statistics*, Chapman & Hall/CRC, Boca Raton, FL.

Montgomery, D.C. (2012), *Design and Analysis of Experiments*, John Wiley & Sons, New York, NY.

Panda, S.K., Padhee, S., Sood, A.K. and Mahapatra, S. (2009), "Optimization of fused deposition modelling (FDM) process parameters using bacterial foraging technique", *Intelligent Information Management*, Vol. 1 No. 2, pp. 89-97.

Patel, J.P., Patel, C.P. and Patel, U.J. (2012), "A review on various approach for process parameter optimization of fused deposition modeling (FDM) process and Taguchi approach for optimization", *International Journal of Engineering Research and Applications*, Vol. 2 No. 2, pp. 361-365.

Roberson, D.A., Espalin, D. and Wicker, R.B. (2013), "3D printer selection: a decision-making evaluation and ranking model", *Virtual and Physical Prototyping*, Vol. 8 No. 3, pp. 201-212.

Roberts, M.J. and Russo, R. (1999), *A Student's Guide to Analysis of Variance*, Routledge, London.

Roy, R.K. (2001), *Design of Experiments using the Taguchi Approach: 16 Steps to Product and Process Improvement*, John Wiley & Sons, New York, NY.

Sood, A.K., Chaturvedi, V., Datta, S. and Mahapatra, S.S. (2011), "Optimization of process parameters in fused deposition modeling using weighted principal component analysis", *Journal of Advanced Manufacturing Systems*, Vol. 10 No. 2, pp. 241-259.

Sood, A.K., Ohdar, R. and Mahapatra, S. (2010), "Parametric appraisal of mechanical property of fused deposition modelling processed parts", *Materials and Design*, Vol. 31 No. 1, pp. 287-295.

Stanek, M., Manas, D., Manas, M., Navratil, J., Kyas, K., Senkerik, V. and Skrobak, A. (2012), "Comparison of different rapid prototyping methods", *International Journal of Mathematics and Computers in Simulation*, Vol. 6 No. 6, pp. 550-557.

Subhani, A. (2011), "Influence of the processes parameters on the properties of the polylactides based bio and eco-biomaterials", PhD thesis, Institut National Polytechnique de Toulouse.

Too, M., Leong, K., Chua, C., Du, Z., Yang, S., Cheah, C. and Ho, S. (2002), "Investigation of 3D non-random porous structures by fused deposition modelling", *The International Journal of Advanced Manufacturing Technology*, Vol. 19 No. 3, pp. 217-223.

Wen, J.-L., Yang, Y.-K. and Jeng, M.-C. (2009), "Optimization of die casting conditions for wear properties of alloy AZ91D components using the Taguchi method and design of experiments analysis", *The International Journal of Advanced Manufacturing Technology*, Vol. 41 Nos 5/6, pp. 430-439.

Yamane, H. and Sasai, K. (2003), "Effect of the addition of poly(d-lactic acid) on the thermal property of poly(l-lactic acid)", *Polymer*, Vol. 44 No. 8, pp. 2569-2575.

Zhang, J.W. and Peng, A.H. (2012), "Process-parameter optimization for fused deposition modeling based on Taguchi method", *Advanced Matarials Research*, Vols 538/539/540/541 No. 1, pp. 444-447.

About the authors

Professor Ali P. Gordon is an Associate Professor in the Department of Mechanical & Aerospace Engineering at the University of Central Florida (Orlando, FL). He directs the Mechanical Properties Characterization Laboratory (MPCL). Prior to joining UCF, he earned a PhD in Mechanical Engineering from the Georgia Institute of Technology (Atlanta, GA). Ali P. Gordon is the corresponding author and can be contacted at: apg@ucf.edu

Jonathan Torres is a Mechanical Engineering PhD candidate at the University of Central Florida in Orlando, FL. He completed his BS and MS at UCF, with his MS work concentrated on the use of ceramic materials for energy conversion, manufacturing and testing solid oxide fuel cells with a unique electrolyte structure. His PhD research is focused on the optimization of material properties as related to the production variables of structures produced via rapid prototyping methods such as FDM and LAM.

Matthew Cole is currently a Mechanical Engineer at Lockheed Martin in Orlando, FL. He earned his BS in Mechanical Engineering from the University of Central Florida in Orlando, FL. During his time there, he participated in both undergraduate and graduate research, which led to his involvement in the design and execution of the research conducted for this paper.

Allen Owji is an undergraduate mechanical engineering student at the University of Central Florida in Orlando, FL. His involvement in the NSF-EXCEL Undergraduate Research Experience program at UCF has allowed him to participate as an Undergraduate Researcher with Dr Ali P. Gordon for a number of semesters. During this time, Allen has become highly proficient at optical microscopy to study fracture surfaces and microstructure such as those presented in this paper.

Zachary DeMastry is an undergraduate mechanical engineering student at the University of Central Florida in Orlando, FL. His high interest in 3D printing and his involvement in the NSF-EXCEL Undergraduate Research Experience program at UCF have allowed him to participate as an Undergraduate Researcher with Dr Ali P. Gordon for a number of semesters. His interest and knowledge in FDM were valuable assets in the design, production and testing of samples for this study.

AUTHOR QUERIES

AUTHOR PLEASE ANSWER ALL QUERIES   1

AQau—Please confirm the given-names and surnames are identified properly by the colours.
    ■= Given-Name, ■= Surname
    The colours are for proofing purposes only. The colours will not appear online or in print.

AQ1— Please provide significance of the bold data in Table IV.